Title: Mineralogy and organic geochemistry of phyllite from the Dewon-Pokrzywna deposit, the Opava Mountains (SW Poland)

Author: Natalia Sawicka, Janusz Janeczek, Monika Fabiańska, Krzysztof Bahranowski, Tomasz Krzykawski, Aniela Matuszewska

Citation style: Sawicka Natalia, Janeczek Janusz, Fabiańska Monika, Bahranowski Krzysztof, Krzykawski Tomasz, Matuszewska Aniela. (2018). Mineralogy and organic geochemistry of phyllite from the Dewon-Pokrzywna deposit, the Opava Mountains (SW Poland). "Geological Quarterly" Vol. 62, iss. 4 (2018), s. 817-828.
doi: 10.7306/gq.1439

Geological Quarterly, 2018, **62** (4): 817–828
DOI: http://dx.doi.org/10.7306/gq.1439

Mineralogy and organic geochemistry of phyllite from the Dewon–Pokrzywna deposit, the Opava Mountains (SW Poland)

Natalia SAWICKA[1], Janusz JANECZEK[1, *], Monika FABIAŃSKA[1], Krzysztof BAHRANOWSKI[2], Tomasz KRZYKAWSKI[1] and Aniela MATUSZEWSKA[1]

[1] University of Silesia, Faculty of Earth Sciences, Będzińska 60, 41-200 Sosnowiec, Poland

[2] Faculty of Geology, Geophysics and Environmental Protection, AGH University of Science and Technology, al. Mickiewicza 30, 30-059 Kraków, Poland

Sawicka, N., Janeczek, J., Fabiańska, M., Bahranowski, K., Krzykawski, T., Matuszewska, A., 2018. Mineralogy and organic geochemistry of phyllite from the Dewon–Pokrzywna deposit, the Opava Mountains (SW Poland). Geological Quarterly, **62** (4): 817–828, doi: 10.7306/gq.1439

Associate editor: Tadeusz Peryt

Phyllites from the Dewon–Pokrzywna deposit in the Opava Mts., SW Poland, were investigated by XRD (Rietveld method), XRF, EPMA, SEM, and ATR-FTIR from the perspective of their potential usage as a buffer and/or backfill material in a geological repository of radioactive waste. Organic matter dispersed in the phyllite matrix was analysed by GC-MS. Fine-grained Mg-Fe-muscovite (13 to 29 wt.%), Fe-ripidolite (10 to 25 wt.%), detrital quartz (20 to 46 wt.%), and albite (7 to 28 wt.%) ± microcline, illite or illite/smectite, and kaolinite are major minerals in phyllite samples. The chlorite/muscovite ratio ranges from 0.65 to 1.1. Mg-annite inherited from the precursor rock is a minor constituent. Detrital ilmenite is a dominant accessory mineral. Ancylite-(Ce) occurs in quartz-calcite-ripidolite veins. Two types of phyllite have been distinguished based on the proportion of phyllosilicates to silt fraction: argillaceous (47 to 55 wt.% phyllosilicates) and silt-rich (28 wt.% phyllosilicates). Argillaceous phyllite shows elevated content of alumina and moderate concentration of silica. It is highly enriched in Fe compared to phyllites from other localities worldwide. The BET specific surface area of argillaceous phyllite ranges from 1.73 to 3.64 m^2/g. Whole-rock chemical composition, mineral assemblages, chlorite geothermometry, and the occurrence of aliphatic hydrocarbons suggest that argillaceous phyllite originated from a pelagic pelite protolith under low-temperature (260–370°C) greenschist to subgreenschist facies conditions. Persistent biomarkers are indicative of bacterial degradation of planktonic organic matter suspended in a high water column. Enrichment in Fe-rich chlorite and Mg,Fe-muscovite, low volume of interconnected pores with dominant mesopores suggest that argillaceous phyllite from the Dewon–Pokrzywna deposit is a potential candidate for a buffer and/or backfill material.

Key words: phyllite, chlorite, organic matter, Dewon Quarry, Poland.

INTRODUCTION

Phyllite is a common foliated, fine-grained rock originated from the low-grade regional metamorphism of pelites. Phyllite is composed mainly of quartz, albite and phyllosilicates: muscovite and chlorite. Phyllites have widely been used for roofing, interior decoration, and in the construction industry. Recently, novel uses have been suggested for crushed or milled phyllites, e.g. fillers in plastics and mortar, barrier material in municipal waste landfills and in cement-based composites (Garzón et al., 2016). Calcinated kaolinized phyllite can be used as a geopolymer resin precursor (Melo et al., 2017). Phyllites have also been proposed as a buffer material for engineering barriers in geological (underground) radioactive waste repositories as an alternative to bentonites (Arnold et al., 1998, 2001; Shahwan and Erten, 1999; Krawczyk-Bärsch et al., 2004). It is the latest usage of phyllites that drew attention of the present authors in search for a cheap and reliable buffer or backfill material to be used in the planned Polish radioactive waste geological repository (Polish Nuclear Power Programme, 2014).

The principal role of a buffer material around waste packages is to protect them from the intrusion of groundwater and, if such an event occurred, to prevent or limit migration of released radionuclides. Currently, bentonite or bentonite mixed with sand is considered the best buffer available (Sellin and Leupin, 2013). However, while bentonite has high sorption capacity, its buffering performance at temperature of 150°C, expected in the near-field of radioactive waste packages, is debatable. Illitization and mechanical degradation of bentonite above 100°C may increase its permeability, though recent experimental works suggest that the net effect of the increased temperature on hydraulic properties of bentonite may be rather small (Daniels et al., 2017). Unlike bentonite, phyllite is thermally sta-

* Corresponding author, e-mail: janusz.janeczek@us.edu.pl

Received: July 13, 2017; accepted: June 5, 2018; first published online: December 3, 2018

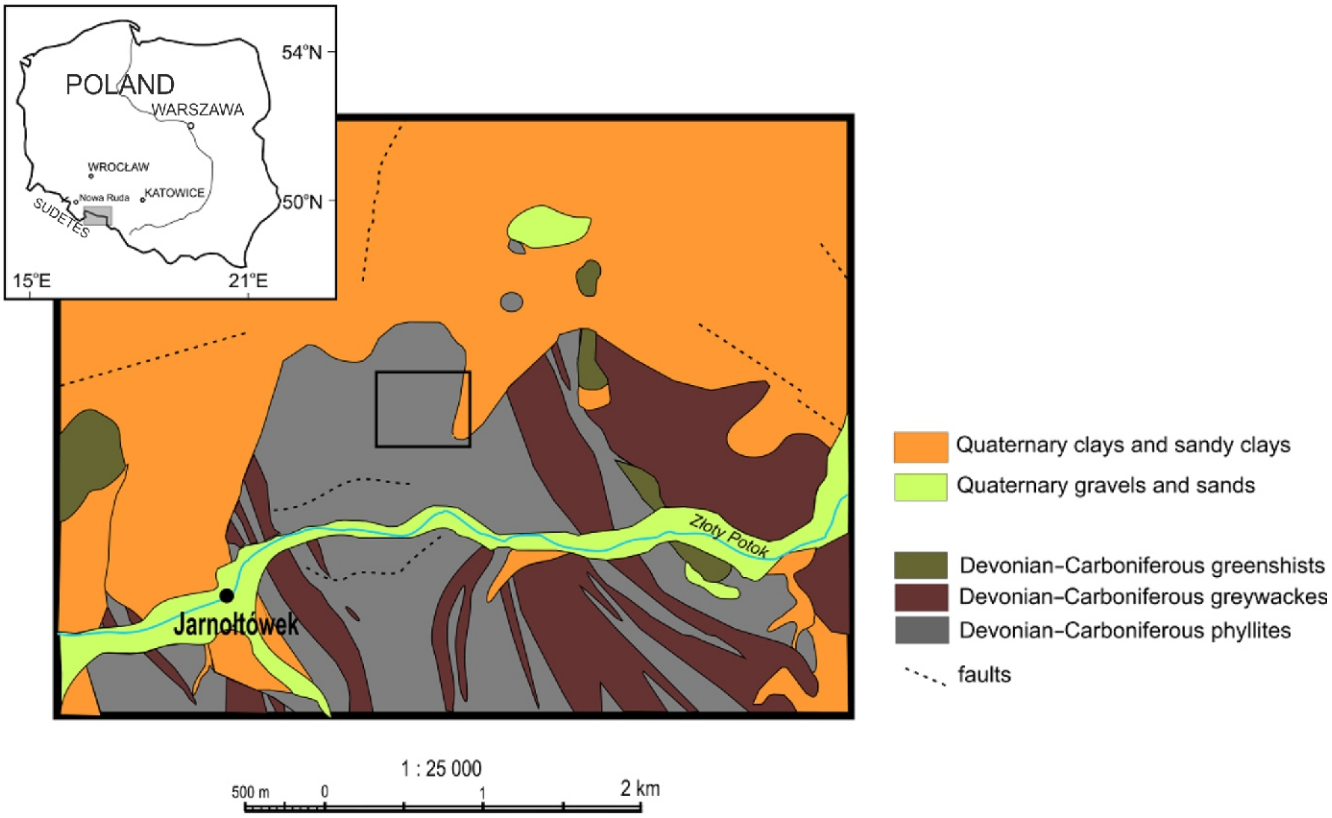

Fig. 1. Simplified geological map of the investigated area in the Polish part of the Opava Mountains (after Sawicki, 1955)

The location of the Dewon–Pokrzywna phyllite deposit and the Dewon Quarry is outlined by the rectangle

ble up to at least 400°C. Thermal stability of phyllite and high sorption capacity for actinides make this rock a potential buffer and/or backfill material either on its own or in a mixture with bentonite. The sorption of radionuclides onto phyllite results primarily from the sorption properties of chlorites and secondary iron oxide hydroxides formed during weathering of chlorites (Arnold et al., 2001; Zänker et al. 2006).

While phyllites in Poland commonly crop out in the Sudetes Mts. and in the Holy Cross Mts., they are quarried only in the Dewon Quarry within the Dewon–Pokrzywna deposit near Jarnołtówek (50.284777N, 17.426419E) in the Polish part of the Opava Mts., Eastern Sudetes (Fig. 1). Up to 90,000 t of slate flour per year are produced and marketed as earth-moist bulk product to be used for road constructions and in the clay bricks and tile industry (Krakow, 2014).

Despite rather simple mineralogy, the variability of both chemical composition and proportions of rock-forming minerals in phyllite samples even from the same locality can be quite high (Garzón et al., 2012, 2016). Therefore, the detailed knowledge of phyllite mineralogy is prerequisite for considering those rocks as a candidate for buffer or backfill material. Despite quarrying phyllites in the Dewon Quarry since 1967 (Słomka et al., 2009), the knowledge on the mineralogy of those rocks is limited (Krakow, 2014; Stańczak, 2016) and is not sufficient to initiate further study needed to determine whether they can be used as a buffer and/or backfill material.

In this paper, we report results of mineralogical investigation of phyllite from the Dewon Quarry. In particular, the focus is on the chemistry of chlorites and white mica because properties of those minerals determine the whole-rock sorption capacity (Arnold et al., 2001; Richter, 2016). Moreover, organic matter dispersed within phyllite was analysed for the first time in search for biomarkers to determine its origin. While carbonaceous phyllites are relatively common, there are only few papers on organic matter in those rocks focused on the organic matter role in the ore-forming processes (Sahoo and Venkatesh, 2014; da Silva Nogueira de Matos et al., 2017).

GEOLOGICAL SETTING

The Dewon–Pokrzywna phyllite deposit occurs at the northern foot of the Opava Mts. in the Polish Eastern Sudetes (Fig. 1). Geologically, the deposit belongs to the Upper Devonian–Lower Mississippian (Famennian–Tournaisian) Andelská Hora unit of the Moravo-Silesian Zone (fold-and-thrust belt on the eastern margin of the Bohemian Massif; Żaba et al., 2005). The Andelská Hora unit is built up of phyllites, metagreywackes, subordinate greenstones (metabasalts), and recrystallized limestone. The flysch-type sedimentary deposits, predominantly alternating slates and sandy (psammitic) slates, were the protolith for the phyllites (Strzyżewska-Konieczna and Żaba, 2002; Stańczak, 2016). Metasandstones and metaconglomerates are interbedded with phyllites. Metaconglomerates contain millimetre- and centimetre-sized pebbles of quartz, metasandstones, slates and limestone. Phyllites were intensely folded and sheared (Fig. 2A) during four major stages of tectonic deformations (Strzyżewska-Konieczna and Żaba, 2002). As a result, chevron folds and crenulation are characteristic features of phyllites in the Dewon–Pokrzywna deposit. The penetrative foliation S_1 developed as schistosity parallel or subparallel to sedimentary bedding S_0. Foliation S_1 was intensely folded during the second stage of tectonic deformation.

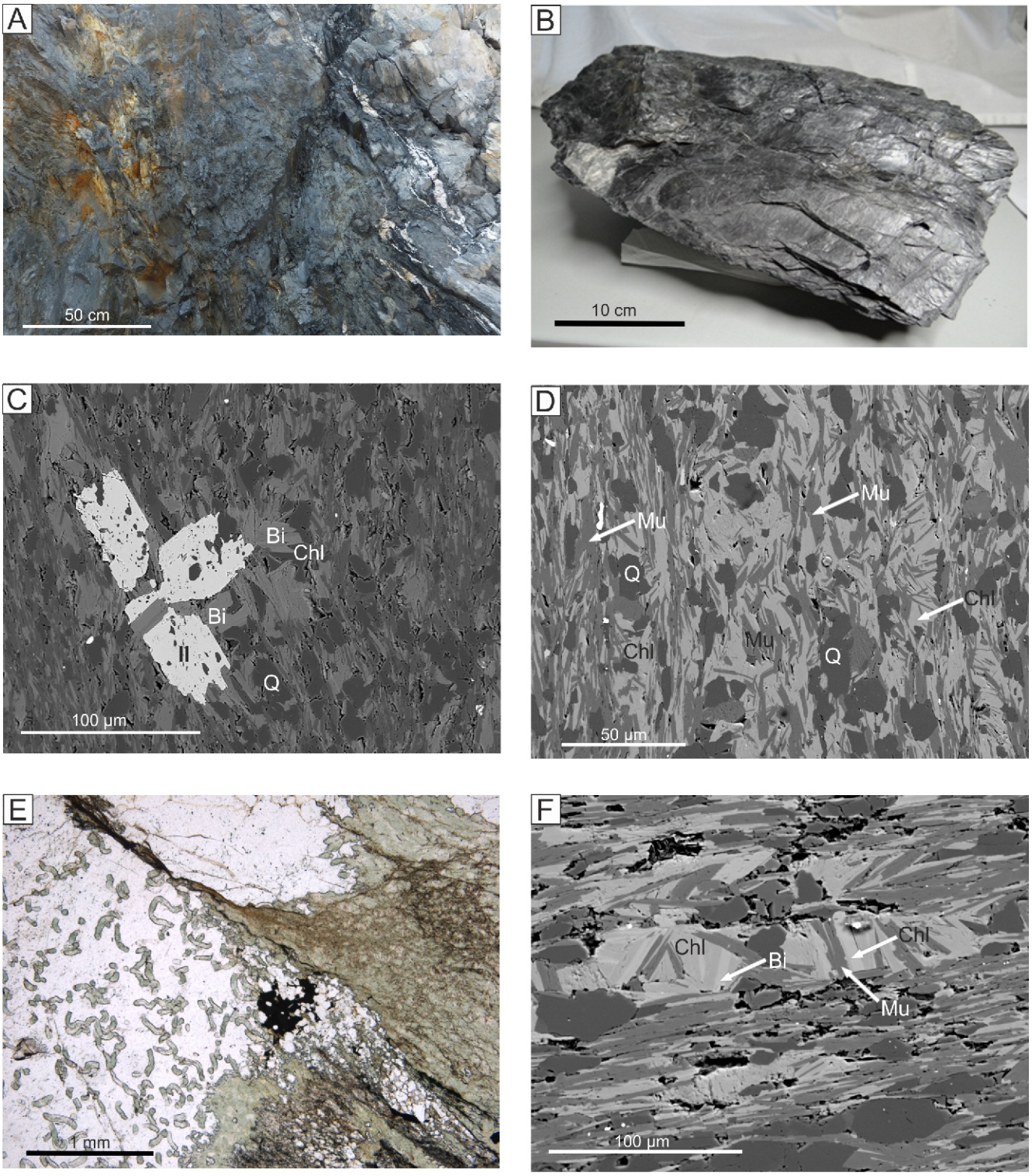

Fig. 2. Phyllites from the Dewon Quarry and their minerals

A – dark grey phyllite exposed in the Dewon Quarry, rusty-brown patches of Fe-oxyhydroxides occur along a shear zone filled with sulphides (pyrite and chalcopyrite), intrafoliated quartz veins occur at the contact with metasandstone (upper right corner), the width of the photograph is 2 m; **B** – hand specimen of phyllite from the Dewon Quarry with a characteristic sheen luster and a quartz vein (lower left side); **C** – BSE image of ilmenite (Il) crystals surrounded by biotite (Bi) (Mg-annite) partially replaced by chlorite (Chl), Q – quartz, ilmenite crystals show embayed grain boundaries and contain quartz inclusions; **D** – BSE image of phyllite, Mu – muscovite; **E** – chlorite aggregates in the quartz-calcite vein in phyllite, plane polarized light; **F** – BSE image of biotite (Mg-annite) aggregate partially replaced by chlorite and overgrown by muscovite, phyllosilicates in the aggregate with cleavage oblique or even perpendicular to foliation

Intrafoliated quartz veins commonly occur within phyllites (Fig. 2A). There are also numerous quartz-calcite (Fig. 2C), quartz, and quartz-albite veins of various thicknesses, crosscutting foliation in phyllites. In some albite veins there are vugs lined with well-developed albite crystals, a few millimetres in size.

SAMPLES AND METHODS

Six samples for this study were collected in the Dewon Quarry. In hand-specimens they are grey, dark grey to almost black and turn light grey with greenish hue in the proximity of quartz veins. Phyllite owes its dark grey colour to carbonaceous matter disseminated more or less evenly throughout the rock. Fraction of millimetre-thick black laminae in phyllite are highly enriched in carbonaceous matter. Foliation surfaces show silky sheen (Fig. 2B). Rusty spots on the phyllite foliation planes are ubiquitous particularly in shear zones filled with sulphides (mostly pyrite and chalcopyrite; Fig. 2A).

Powdered phyllite samples were analysed using a *Pananalytical X'Pert PRO-PW 3040/60* X-ray diffractometer (CuK $_1$ source radiation, Ni-filter to reduce the K radiation, and X'Celerator detector). Quantitative data processing was performed by means of the *X'PERT High Score Plus* software using the latest PDF4+ database and applying the Rietveld method.

Whole-rock chemical composition of phyllite samples was determined by wavelength dispersive X-ray fluorescence (WD-XRF) of fused samples using the *WD-XRF ZSX Primus II Rigaku* spectrometer with Rh anode. Samples were melted in the presence of fluxing agent (66.67% $Li_2B_4O_7$, 32.83% $LiBO_2$, 0.5% LiBr) with the sample to fluxing agent ratio of 1:9. Semi-quantitative analyses were performed using the *SQX Calculation* software (fundamental parameters method).

Chemical compositions of minerals in samples JN1, JN2, and JN4 were determined at the Inter-Institute Laboratory for the Microanalysis of Minerals and Synthetic Materials (Faculty of Geology, University of Warsaw) using a *CAMECA SX-100* microprobe operated in the wavelength-dispersive (WDS) mode at an accelerating voltage of 15 kV and a sample current of 10–20 nA. The beam diameter was 10 μm. The following standards were used: albite for Na, diopside for Si, Mg and Ca, orthoclase for Al and K, Fe_2O_3 for Fe, rhodonite for Mn, and rutile for Ti.

Samples were observed by SEM using a *Philips XL 30 ESEM/TMP* scanning electron microscope coupled with an energy-dispersive spectrometer (EDS; EDAX type Sapphire) at the Faculty of Earth Sciences, University of Silesia under the following operating conditions: accelerating voltage 15 kV; working distance ~10 mm; counting time 40 s. The same conditions were applied for back-scattered electron (BSE) imaging.

Attenuated total reflection-Fourier transform infrared (ATR-FTIR) spectra were obtained from finely powdered samples on a *Nicolet iS10 Mid FT-IR* Spectrometer (Thermo Scientific) fitted with an ATR device with a diamond crystal plate. Samples were placed directly onto the diamond crystal prior to data acquisition. Measurement conditions were: spectral range 4000–400 cm^{-1}, spectral resolution 4 cm^{-1}, beam splitter Ge/KBr, detector *DLaTGS* with dynamic interferometer justification. The *OMNIC 9* (Thermo Fisher Scientific Inc.) analytical software was used.

The surface area and pore structure were determined from nitrogen adsorption/desorption isotherms at liquid nitrogen temperature (–196°C) using *Micrometrics ASA2020* equipment under a relative pressure range of 10^{-3} to 0.99. Samples were heated in vacuum at 150°C for 12 hours prior to measurements. A standard Braunaer-Emmet-Teller (BET) methodology (ISO 9277:2010) was applied for the specific area estimates.

Density (D) of bulk powdered samples was measured with a pycnometer using toluene (D = 0.872 gcm^{-3} at 23°C). Density of each sample was determined three times and the results were averaged.

Total carbon (TC), total inorganic carbon (TIC), and total sulphur (TS) were determined using an *Eltra CS-500 IR-analyzer* with a TIC module. TC, TS and TIC contents were measured using an infrared cell detector of CO_2 and SO_2 gases, which was evolved by combustion under an oxygen atmosphere for TC and TS, respectively, and was obtained from reaction with 10% hydrochloric acid for TIC. Total organic carbon (TOC) was calculated as the difference between TC and TIC. Calibration was made by means of Eltra standards. Calcium carbonate content was calculated as $CaCO_3$ = 8.333 TIC, assuming that all carbonate occurs as calcite.

Approximately 16 g aliquots of each sample were extracted with dichloromethane (DCM) using the *Dionex 350 Accelerated Solvent Extractor* system (Thermo Scientific) at 70°C in 34 ml stainless steel cells (P = 10 MPa, solvent flow = 70 ml/min, extraction time 15 min.). Copper mesh was applied to remove elementary sulphur from the extracts. Solvent was evaporated at room temperature and dried extracts were weighted to calculate extraction yields (wt.%). Dry residue was diluted in 0.5 ml of DCM and analysed with GC-MS. All solvents and reagents were pure for analysis grade (Avantor Performance Materials Poland S.A.).

An Agilent gas chromatograph 7890A with a DB-5 column (60 m 0.25 mm i.d.), coated by a 0.25 μm stationary phase film coupled with an Agilent Technology mass spectrometer *5975C XL MDS* was used. The experimental conditions were: carrier gas – He; initial temperature 50°C (isothermal for 2 min); heating rates: to 175°C at 10°C/min, to 225°C at 6°C/min, and to 300°C at 4°C/min. The final temperature (300°C) was held for 20 min. The mass spectrometer was operated in the electron impact ionisation mode at 70 eV and scanned from 50 to 650 da. Data were acquired in a full scan mode and processed with the *Hewlett Packard Chemstation* software. The chemical compounds were identified based on their mass spectra, comparison of peak retention times with standards, interpretation of MS fragmentation patterns, and literature data (Philp, 1985; Wiley, 2014). Analysed mass ions include: m/z = 71 for *n*-alkanes, m/z = 183 for acyclic isoprenoids, m/z = 191 for pentacyclic triterpenes, m/z = 217 for steranes, m/z = 142, 156, 170 and 184 for alkyl naphthalenes, m/z = 192, 206, and 220 for alkyl phenanthrenes.

RESULTS

MINERAL COMPOSITION

Phyllite from the Dewon Quarry is composed of quartz, muscovite, chlorite and albite as major (>5 wt.%) constituents (Table 1). Additionally, kaolinite, microcline, and illite or illite/smectite, and a mixed-layer clay mineral, possibly chlorite/smectite are among major minerals in sample JN1 (Fig. 3). Biotite occurs in some samples as a minor constituent. Calcite occurs as intrafoliated grains and veinlets crosscutting phyllite. Ilmenite (Fig. 2C), zircon, apatite, titanium oxide, allanite, monazite, xenotime, pyrite, chalcopyrite and unidentified As-sulphosalts of Co and Fe are detrital accessory minerals.

Table 1

Mineral composition (wt.%) and density (gcm^{-3}) of phyllites from the Dewon Quarry

Sample	Chlorite	Muscovite	Chlo/Mu	Quartz	Albite	Biotite	Kaolinite	Microcline	Density
JN1*	10	13	0.77	26	11	–	16	14	2.61
JN2	22	34	0.65	20	24	–	–	–	2.57
JN3	18	28	0.64	25	28	1	–	–	2.52
JN5	25	29	0.86	21	20	–	4	1	2.56
JN4**	19	28	0.68	26	7	–	–	–	2.46
JN6	15	13	1.15	46	26	–	–	–	2.52

*JN1 contains additionally 10 wt.% of illite or illite/smectite and subordinate mixed-layer clay mineral tentatively identified as chlorite/smectite; **JN4 contains 20 wt.% calcite, perhaps as an impurity from calcite veinlets

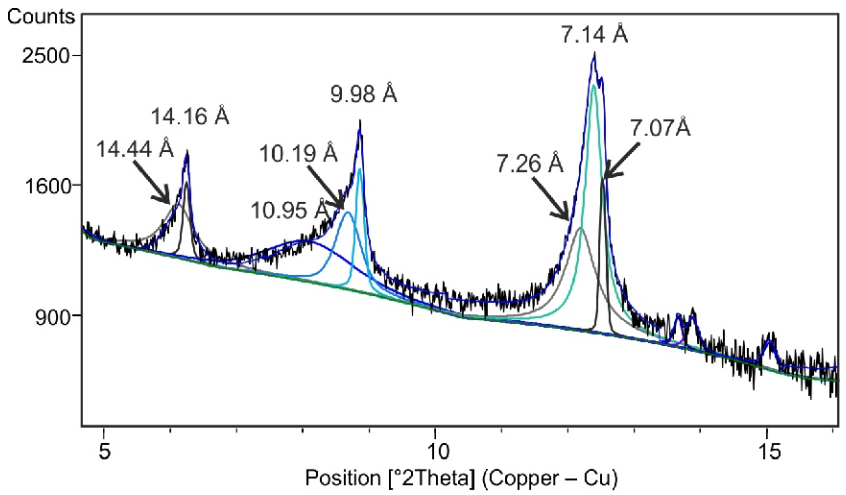

Fig. 3. X-ray powder diffraction pattern of phyllite (sample JN1) from the Dewon Quarry showing deconvoluted basal reflections from phyllosilicates

Chlorite (sharp and strong peaks at 14.16 Å and 7.07 Å), muscovite (sharp and strong peak at 9.98 Å), kaolinite (very strong and broad peak at 7.14 Å), illite or illite/smectite (very broad peak at 10.19 Å), and a mixed-layer silicate, possibly chlorite/smectite (very broad peaks at 14.44 Å and 7.26 Å)

Elongate, lenticular quartz grains (clasts) are up to ~100 μm long and ~50 μm thick. They are aligned parallel to foliation. Albite grains are of similar size, but unlike quartz they are angular and apparently less plastically deformed. Muscovite and chlorite are intimately intergrown (Fig. 2D), though some observations suggest that chlorite overgrowths muscovite. There are two generations of chlorite: the fine-grained one in the phyllite matrix, and coarse aggregates within calcite-quartz veins that crosscut phyllite (Fig. 2E). The latter generation shows anomalous indigo-blue interference colours under the polarizing microscope.

Aggregates of biotite partially replaced by chlorite have cleavage oblique or even perpendicular to foliation (Fig. 2F). They are primary clasts as suggested by interpretation of similar biotite "stacks" in slates and phyllites from other localities (Vernon, 2004).

Ilmenite is the ubiquitous accessory mineral. It is often intergrown with quartz and displays features indicative of partial dissolution, i.e. its grain boundaries are embayed and irregular (Fig. 2C). Some of its grains are fragmentized apparently due to mechanical deformations. Ilmenite is frequently associated with biotite. Ancylite-(Ce), ideally $CeSr(CO_3)_2(OH) \cdot H_2O$, was observed in quartz-calcite veins crosscutting phyllite sample JN1B. To our knowledge, this is the first occurrence of this relatively rare mineral in the Sudetes Mts.

Phyllite-forming minerals occur in various proportions in the investigated samples, as revealed by the Rietveld method (Table 1). The amount of quartz ranges from 20 to ~46 wt.% in the most psammitic phyllite (JN6). The average amount of quartz in samples JN1 to JN5 is ~ 24 ± 3 wt.%. The amount of albite ranges from 11 to almost 28 wt.%. Samples show variable concentrations of chlorite and muscovite from 10 to ~26 wt.% and from 11 to 34 wt.%, respectively. The chlorite to muscovite ratio ranges from 0.65 to 1.10; however, muscovite is a predominant phyllosilicate in the majority of samples. Sample JN1 (Table 1) shows signs of significant weathering, as suggested by the occurrence of illite and kaolinite. This particular sample is also enriched in K-feldspars (~14 wt.%) and is relatively depleted in albite (11 wt.%). There is a negative linear correlation between the amount of quartz and the amount of phyllosilicates (not shown in the paper). The most psammitic sample (JN6) contains 46 wt.% of quartz and the lowest amount of phyllosilicates (28 wt.%) with chlorite slightly predominant over muscovite. That sample is also enriched in albite. The difference in the mineral quantitative composition of phyllite samples most likely reflects the variability of the protolith. The argillaceous protolith

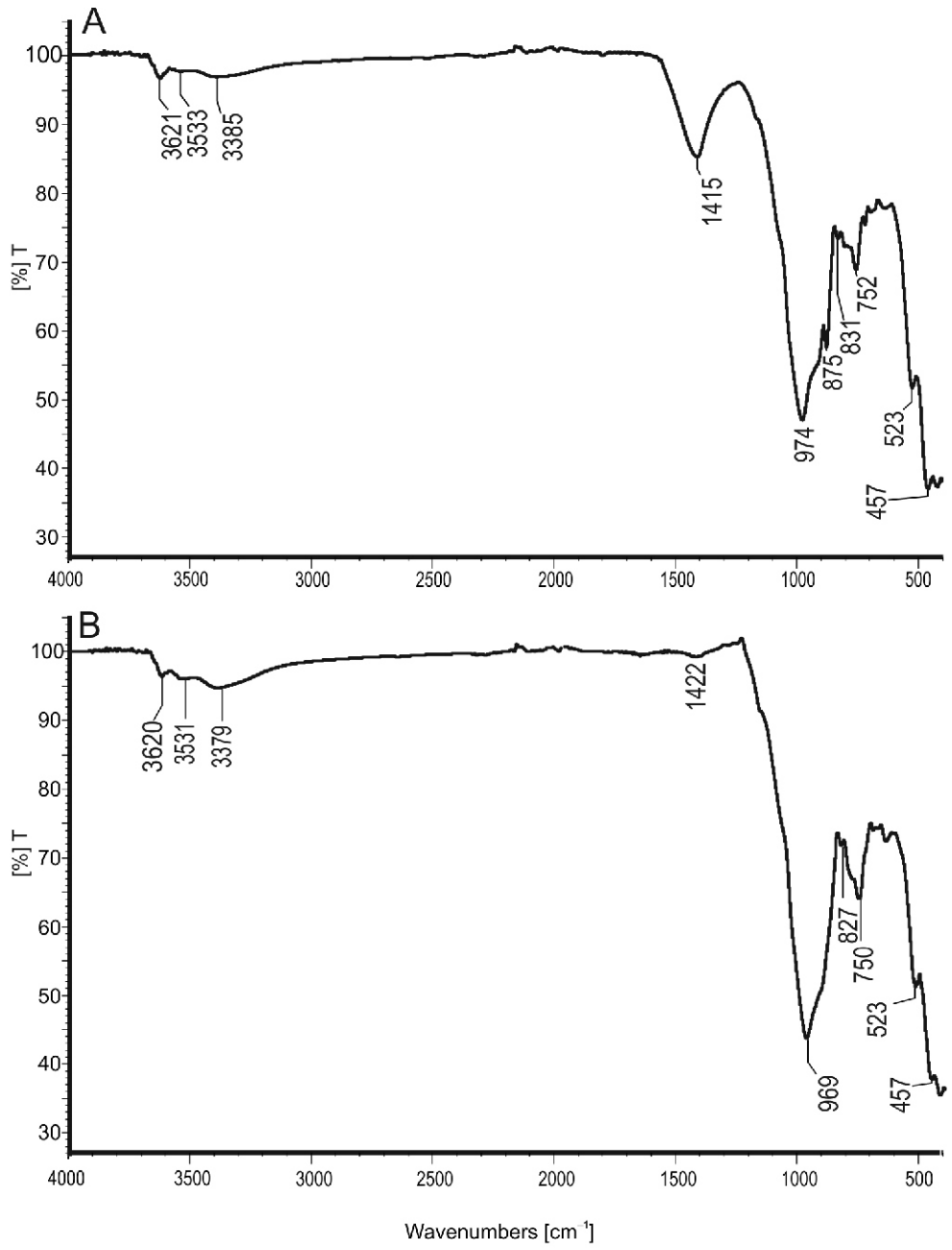

Fig. 4. FT-IR spectra of phyllite samples JN4 (A) and JN2 (B)

turned into muscovite-chlorite-rich assemblages; whereas, the higher silt fraction reflects a psammitic protolith.

FT-IR spectra (Fig. 4) confirm the general similarity of all phyllite samples due to their similar mineralogical composition with the exception of sample JN4, which contains calcite (bands at 1415 and 875 cm^{-1} in Fig. 4A), and sample JN6, which is quartz-dominant (there is a double band characteristic of quartz at 798-779 cm^{-1} in the FT-IR spectrum of JN6). In the OH spectral range, the strongest band at 3620 cm^{-1} is most probably associated with the stretching vibrations of OH groups located within octahedral sheets of layered silicates (Balan et al., 2001). The strongest band at 969–974 cm^{-1} results from the Si-O stretching vibrations.

The BET specific surface area (S_{BET}) of argillaceous phyllite ranges from 1.73 m^2/g (JN2) to 3.64 m^2/g (JN5). The S_{BET} value of 0.5 m^2/g for the most psammitic sample (JN6) is an order of magnitude lower as a result of the lowest amount of phyllosilicates. However, there is no simple correlation between S_{BET} and the amount of phyllosilicates in argillaceous phyllite samples. Samples JN2 and JN5 with the highest quantity of phyllosilicates (55 and 54 wt.%, respectively) have an extremely different specific surface area, as shown above. Possibly, textural features of those samples determine their specific surface area. While sample JN2 has the lowest pore volume (0.007 cm^3/g for p/p^0 = 0.99), sample JN5 has the highest (0.010 cm^3/g). Even the highest S_{BET} value for the investigated phyllites is twice less the S_{BET} value (7.6 m^2/g) measured in clay phyllite from Spain, containing up to 75% of phyllosilicates (illite/muscovite plus chlorite; Garzón et al., 2010).

Pore size distribution in all of the investigated argillaceous phyllite samples is similar. Mesopores (pores in the range of 2–50 nm) are dominant, ranging from 56 to 60% of the total

Table 2

Chemical composition (wt.%) of phyllite samples from Jarnołtówek

	JN1	JN2	JN3	JN5	Pelites*	JN6
SiO_2	54.63	55.36	55.49	52.71	54.9	67.62
TiO_2	1.12	1.02	1.23	1.29	0.8	0.99
Al_2O_3	19.47	19.98	19.77	20.63	16.6	14.20
$Fe_2O_3^{\#}$	9.63	9.57	9.69	9.17	9.9	5.53
MnO	0.23	0.19	0.16	0.19	–	0.12
MgO	2.98	3.09	2.75	2.49	3.4	1.54
CaO	1.63	0.78	0.55	0.60	0.7	1.85
Na_2O	2.03	2.04	3.16	2.01	1.3	2.87
K_2O	2.98	3.66	3.19	3.81	2.7	1.97
P_2O_5	0.16	0.20	0.22	0.20	–	0.17
SO_3	0.05	0.09	0.05	0.03	–	0.17
L.O.I	4.51	3.80	3.54	4.09	9.2	2.90
Total	99.37	99.69	99.75	97.19	99.5	99.76
f	0.79	0.78	0.80	0.81	0.77	0.81
Si/Al	2.39	2.36	2.36	2.22	2.75	4.04
Na/K	1.05	0.85	1.56	0.83	0.67	2.21

L.O.I – loss of ignition; f = Fe/(Fe + Mg); # – as total Fe; * – Bucher and Grapes (2011); trace elements detected during XRF analysis: Cu, Ni, Rb, Sr and V

pore volume. Micropores (pores with free diameter <2 nm) occupy between 11 and 14%, and macropores (>50 nm) range from 29 to 37% of the total pore volume.

Density of phyllite samples ranges from 2.46 to 2.61 gcm^{-3} (Table 1). There is no obvious correlation between the mineral composition and the measured density. However, the highest density recorded in sample JN1 may be due to its enrichment in heavy accessory minerals compared to other samples. Density measured during this study is lower than that reported in the literature (2.68 gcm^{-3}; Stańczak, 2016).

WHOLE-ROCK CHEMICAL COMPOSITION

All of the investigated samples with the exception of JN6 have similar bulk chemical compositions (Table 2). Sample JN6 is enriched in silica and depleted in other elements as a result of the high amount of quartz (Table 1). The variation in silica content of up 2.8 wt.% is inversely correlated with the concentration of alumina reflecting the changes in the quartz to aluminosilicates ratio. With the exception of the most psammitic sample JN6, phyllite samples show negligible variation in the Si/Al atomic ratio (Table 2).

While by weight, K predominates over Na, the atomic proportions of Na and K (Na/K) almost directly reflect the proportions between albite and muscovite and, in the case of sample JN1, between albite and both muscovite and microcline.

Relatively high concentrations of Ti compared to low concentrations of this element in chlorite and muscovite suggest accessory ilmenite as a major carrier of Ti. While biotite is significantly enriched in TiO_2 (on average 1.68 wt.%; Appendix 1*), its amount is too low to account for the Ti concentrations in the phyllite samples. Increased concentrations of Ca in samples JN1 and JN6 result from intrafoliated calcite grains. Accessory apatite may only insignificantly contribute to the Ca concentration in whole-rock, because of its scarcity in phyllite.

All samples are ferruginous and are enriched in Fe relative to Mg, as indicated by the high values of the Fe/(Fe + Mg) ratio averaged at 0.80 (Table 2). Loss of ignition reflects the relatively high concentration of water in rock-forming phyllosilicates.

Overall, the chemical composition of argillaceous phyllite from the Dewon Quarry resembles the average chemical composition of pelagic pelites (Table 2). The notable differences include higher Si/Al ratio and lower Na/K ratio in the latter. Much lower content of water in phyllite samples compared to pelites can simply be explained by water loss during pelites metamorphism.

MINERAL CHEMISTRY

Chlorite. All of the investigated chlorites have similar chemical compositions (Appendix 1). In particular, there is no significant difference between chlorite from the rock groundmass and the one from quartz-calcite veins. The deviation from the median value for all cations is in the range of 0.04 to 0.14 atoms per formula unit (apfu). All chlorites are Fe-dominant with Fe/(Fe+Mg) ranging from 0.55 to 0.58. Iron in chlorites is apparently divalent, as suggested by charge balance in crystal chemical formulae. The deficiency in octahedral sites calculated from EPMA (Appendix 1) may result from: (a) analytical errors, (b) vacancies, and (c) the occurrence of some Fe^{3+}. No attempt was made to calculate the latter due to uncertainty in the cause of the octahedral site deficiency.

All of the investigated rock-forming chlorites are slightly peraluminous (Si/Al in the range of 0.94 to 0.97), while one of the analysed chlorites from the calcite veinlets (JN1 vein in Appendix 1) has the Si/Al ratio of 1.02. The general crystal-chemical formula of chlorite based on data in Table 2 is:

* Supplementary data associated with this article can be found, in the online version, at doi: 10.7306/gq.1439

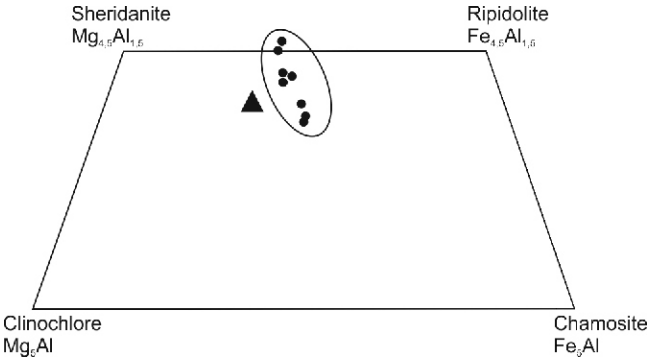

Fig. 5. Diagrammatic representation of chemical compositions of chlorites octahedral sheets

dots – Dewon Quarry; triangle – Grimsel, Switzerland (chlorite used in sorption experiments by Arnold et al., 1998); classification scheme of Mg-Fe-Al chlorites from Wiewióra nad Weiss (1990)

$(Fe^{2+}_{2.4–2.6}Mg_{1.9–2.0}Al^{VI}_{1.4–1.5})_{5.7–6.01}(Si_{2.6–2.7}Al^{IV}_{1.4–1.3})O_{10}(OH)_8$. According to the classification by Wiewióra and Weiss (1990), the investigated chlorites belong to the ripidolite $(Fe^{2+}_{4.5}Al_{1.5})(Si_{2.5}Al_{1.5})O_{10}(OH)_8$ – sheridanite $(Mg_{4.5}Al_{1.5})(Si_{2.5}Al_{1.5})O_{10}(OH)_8$ series, with the ripidolite molecule (56%) slightly dominated over the Mg end-member (Fig. 5).

Unit cell parameters of phyllite-forming chlorites were calculated using the Rietveld method for the C2/m (12) space group (Appendix 2). All of the investigated chlorites crystallize in the IIb polytype. The maximum difference in unit cell parameters varies from 0.02 Å for *c* parameter to 0.04 Å for *a* parameter, which translates into the maximum difference of 2.5 $Å^3$ in volume of the unit cell. Those differences are most probably caused by small differences in chemical compositions of chlorite from various samples, but they can be considered insignificant.

Micas. EPMA data for muscovite and biotite are given in Appendix 1. Based on charge balance calculations, Fe in muscovite is divalent. The averaged crystal chemical formula of muscovite is $K_{0.88}\ Na_{0.04}\ (Fe^{2+}_{0.13}\ Mg_{0.15}\ Ti_{0.02}\ Al_{1.74})_{2.04}\ [(Si_{3.24}\ Al_{0.76})_{4.00}\ O_{10.00}]\ (OH)_{2.00}$. According to the classification of Tischendorf et al. (2007) the investigated white mica can be classified as Mg-Fe muscovite of the muscovite-phengite series, in which some 14% of octahedral sites is occupied by Mg and Fe (Mg+Fe = 0.27 apfu.). Contrary to chlorites, Mg slightly dominates over Fe (Mg/(Mg+Fe) = 0.54) in muscovite. Muscovite from the Dewon Quarry is tetrahedral Al-deficient compared to ideal muscovite, in which the Al/Si is 1:3.

Unit cell parameters of muscovite are remarkably similar in almost all samples and are as follows: *a* = 5.202 Å, *b* = 9.022 Å, *c* = 20.063 Å, = 95.746°. Muscovite in sample JN1 has slightly lower unit cell parameters except for the angle: *a* = 5.185 Å, *b* = 9.000 Å, *c* = 20.043 Å, = 95.984°.

The averaged crystal chemical formula of biotite is $K_{0.76}\ Na_{0.01}\ (Fe^{2+}_{1.42}\ Mg_{1.01}\ Ti_{0.10}\ Al_{0.41}\ Mn_{0.01})_{2.95}\ [(Si_{2.70}\ Al_{1.30})_{4.00}\ O_{10.00}]\ (OH_{2.00})$. The ratio of Fe/(Fe+Mg) = 0.58 is similar to the average ratio observed in the investigated chlorites (0.57). "Biotite" is a series name applied to dark micas compositionally between or close to the annite-phlogopite and siderophyllite-eastonite end-members (Rieder et al., 1998) To classify properly dark mica from the Jarnołtówek phyllite we used simple parameters proposed by Tischendorf et al. (2007), i.e. *mgli* = Mg – Li and *feal* = $^{VI}(Fe_{tot}+Mg+Ti) – {}^{VI}Al$ (apfu). From data in Table 3, biotite from the Jarnołtówek samples can be classified as a member of the annite $(KFe^{2+}[AlSi_3O_{10}](OH)_2)$ – phlogophite $(KMg[AlSi_3O_{10}](OH)_2)$ series with the annite component of 58% mol. and with $^{VI}Al < 0.5$ (mgli = 1.01, feal = 2.11). Applying the 50/50 rule for mineral series (solid solutions), the dark mica in the investigated phyllite is Mg-rich annite and this name will be used further on in this paper. Annite is partially replaced by chlorite (Fig. 2F).

ORGANIC GEOCHEMISTRY

Organic matter is finely dispersed throughout phyllite samples. Isolated organic nodules have not been observed under SEM. Those observations suggest the amorphous type of organic matter typical for either marine or lacustrine origin.

Total Carbon (TC) content in phyllites is related to the amount of calcite (except for samples JN2 and JN3) and varies from 0.386 to 2.651 wt.%. Total Organic Carbon (TOC) and extract yields in all of the phyllite samples are very low and range from 0.012 to 0.44 wt.% and from 0.002 to 0.015 wt.%, respectively (Table 3). However, even such a low concentration of extractable bitumen in phyllites is rather unusual because organic matter in metamorphic rocks is highly overmature. There

Table 3

Concentration (wt.%) of total sulphur, various forms of carbon, and carbonates, and extract yield and values of biomarker ratios of phyllite samples from the Dewon Quarry

Sample	TC	TS	TIC	TOC	CC	Extract yield	1	CPI	Pr/Ph	Pr/*n*-C_{17}	Ph/*n*-C_{18}
JN1	0.67	0.01	0.228	0.44	1.90	0.015	0.33	1.15	0.51	0.33	0.19
JN2	0.39	0.02	0.0	0.39	0.0	0.005	0.72	1.00	0.49	0.32	0.26
JN3	0.42	0.11	0.0	0.42	0.0	0.007	0.62	1.22	0.55	0.32	0.22
JN4	2.65	0.04	2.64	0.01	22.10	0.014	0.40	1.10	0,50	0.40	0.27
JN5	0.40	0.01	0.02	0.38	0.15	0.012	0.70	1.05	0.41	0.34	0.27
JN6	0.46	0.07	0.14	0.33	1.15	0.002	0.48	1.20	0.61	0.38	0.27

TC – total carbon, TS – total sulphur, TIC – total inorganic carbon, TOC – total organic carbon, CC – carbonate content; 2/ 1 = [(from *n*-C_{23} to *n*-C_{37})]/[(from *n*-C_{11} to *n*-C_{22})], *m/z* = 71, source indicator (Tissot and Welte, 1984); Carbon Preference Index (CPI) = 0.5{[(*n*-C_{25}+*n*-C_{27}+*n*-C_{29}+*n*-C_{31}+*n*-C_{33})/(*n*-C_{24}+*n*-C_{26}+*n*-C_{28}+*n*-C_{30}+*n*-C_{32})]+[(*n*-C_{25}+*n*-C_{27}+*n*-C_{29}+*n*-C_{31}+*n*-C_{33})/(*n*-C_{26}+*n*-C_{28}+*n*-C_{30}+*n*-C_{32}+*n*-C_{34})], *m/z* = 71, thermal maturity parameter (Bray and Evans, 1963); Pr/Ph = pristane/phytane, parameter of environment oxicity (excluding coals), *m/z* = 71 (Didyk et al., 1978); Pr/*n*-C_{17} = pristane/*n*-heptadecane, *m/z* = 71 (Leythauser and Schwartzkopf, 1985); Ph/*n*-C_{18} = phytane/*n*-octadecane, *m/z* = 71 (Leythauser and Schwartzkopf, 1985)

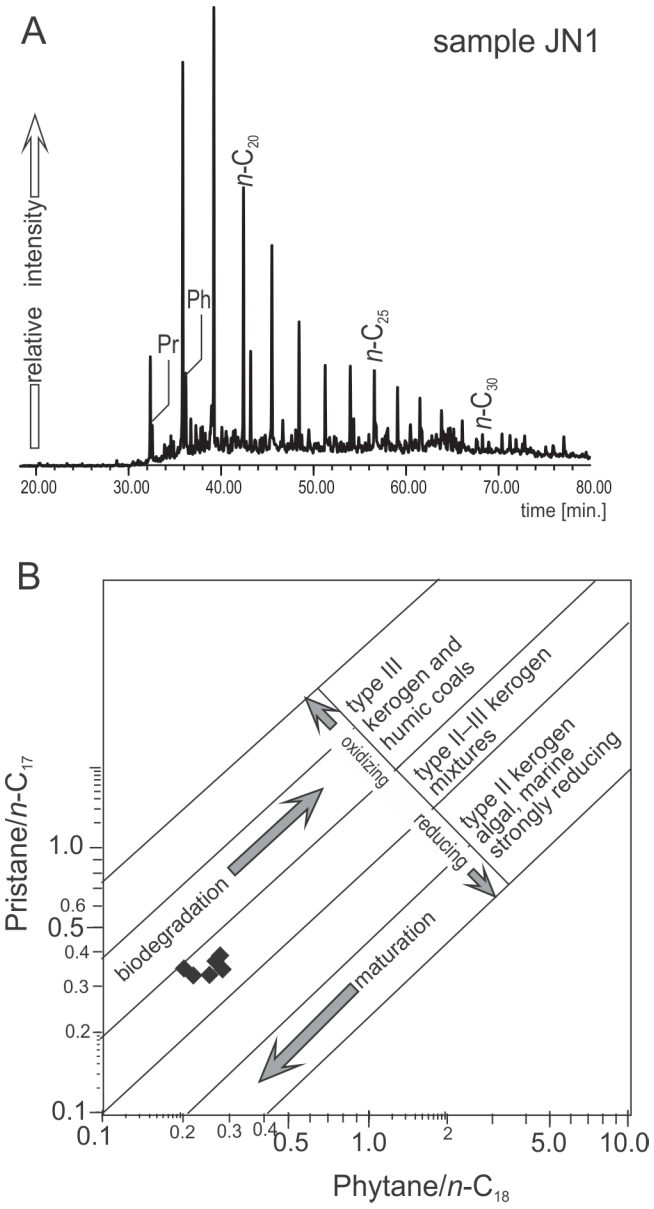

Fig. 6A – *n*-alkanes distribution in phyllite extracts, ion chomatogram *m/z* = 71; B – pristane/*n*-C_{17} *versus* phytane/*n*-C_{18} diagram showing geochemical features of organic matter in phyllite from the Dewon Quarry, genetic categories after Shanmugam (1985), Pr – pristane, Ph – phytane

is no obvious correlation between TOC and the extract yield, possibly due to contamination by both elemental sulphur (S_8) not entirely removed from extracts and recent organic compounds of biological origin, such as fatty acids (roughly 70–90% of the extract, as estimated from peak areas on the Total Ion Chromatogram).

Low amount of organic matter hindered its FT-IR analysis. Only a weak absorption band at ~1600 cm^{-1} in the spectra of samples JN1 and JN2 may be attributed to the C = C bonds.

Organic portions of the extracts display features typical of overmature sedimentary organic matter (Peters et al., 2005). They consist of series of predominant *n*-alkanes, a few alkylcyclohexanes, and two acyclic isoprenoids: pristane (Pr) and phytane (Ph). All other biomarkers and aromatic hydrocarbons were thermally destroyed under the greenschist facies conditions, i.e. at temperatures up to 365°C (see the geothermometry section below). The lack of biomarkers caused by the organic matter graphitization has been observed in metamorphic rocks worldwide (e.g., Van Zuilen et al., 2003; Kříbek et al., 2008).The widest *n*-alkane distribution comprises compounds in the range of *n*-C_{16}-*n*-C_{27} (JN1) and the narrowest *n*-C_{17}-*n*-C_{23} (JN4). The outline of distribution is smooth without any odd-over-even carbon number atom domination. Values of the Carbon Preference Index (CPI), which is a numeric expression of odd-over-even carbon number predominance, calculated from the formula of Bray and Evans (1963), are ~1.0 (Fig. 6A and Table 3). Maximum of the distribution falls to *n*-C_{19} in all samples. All of those features are common in plankton-originated organic matter, possibly partially biodegraded, since *n*-alkanes lighter than *n*-hexadecane were removed in all samples (Fig. 6A). Calculated Pr/*n*-C_{17} and Ph/*n*-C_{18} ratios are low, on average 0.36 and 0.24, respectively. Extremely low values of both indices are caused by high maturity of organic matter. When plotted on the Pr/*n*-C_{17} *versus* Ph/*n*-C_{18} diagram (Fig. 6B) they indicate both low oxygen content in the depositional environment and type II/III kerogen of high maturity. Such kerogen, i.e. organic matter of mixed algal and terrestrial origin, is common in marine sedimentary environments, e.g. within continental shelves (Leythauser and Schwartzkopf, 1985; Summons et al., 1988; Cooper, 1990). Terrestrial organic matter may be deposited in the continental shelves and mix with planktonic organic matter formed *in situ*. However, phytoclasts were not observed under SEM, possibly due to organic matter scarcity in the investigated rocks and/or its very fine dispersion.

Values of the Pr/Ph ratio are similar in all samples (0.41–0.61; Table 3) and indicate the anoxic environment during the organic matter deposition (Didyk et al., 1978).

GEOTHERMOMETRY

Chemical composition of chlorite can be used to estimate its crystallization temperature based on the observation of systematic increase in ^{IV}Al with increasing temperature. Various empirical chlorite geothermometers have been proposed (Yavuz et al., 2015 and references therein). The chlorite crystallization temperature in phyllite from the Dewon Quarry, calculated using six of those geothermometers and chemical data (Table 2), ranges from as low as 242 up to 372°C (Table 4). The most commonly used geothermometer of Cathelineau (1988) gives 298 ± 6°C. All of the empirical chlorite geothermometers suffer from numerous uncertainties, and thus no single chlorite geothermometer provides a reliable temperature (De Caritat et al., 1993). The chemical composition of chlorite depends not only on temperature but also on other thermodynamic parameters of the crystallization system. Nevertheless, the temperature range calculated for chlorite from phyllite samples is consistent with the low-temperature greenschist or high-temperature subgreenschist facies typical of the phyllite formation.

The occurrence of aliphatic hydrocarbons in the phyllite extracts suggests that the peak temperature during metamorphism did not exceed 270°C, since this is a threshold value above which aliphatic hydrocarbons are thermally destroyed (Clifton et al., 1990). However, some observations suggest that *n*-alkanes can survive even under the greenschist facies conditions (Oruzinsky and Kribek, 1981) and this seems to be the case in phyllites from the Dewon–Pokrzywna deposit.

Table 4

Chlorite crystallisation temperature (°C) calculated from various empirical geothermometers

Sample	Geothermometers					
	1	2	3	4	5	6
JN1a	298	341	364	277	308	252
JN1b	297	339	362	276	308	251
JN2a	288	329	348	268	296	242
JN2b	304	345	372	283	318	258
JN4	304	346	372	282	316	257
Average	298	340	364	277	309	252
JN1vein	292	335	354	270	297	245
JN1vein	309	351	380	288	324	263
Average	300	343	367	279	310	254

Detailed references to the listed authors are in Yavuz et al. (2015): 1 – Cathelineau and Nieva (1985); 2 – Kranidiotis and MacLean (1987); 3 – Kavalieris et al. (1990); 4 – Zang and Fyfe (1995); 5 – Xie et al. (1997); 6 – El-Sharkawy (2000)

DISCUSSION

Review of available data on phyllite chemical and mineral compositions reveal that under the name phyllite, authors report rocks with a very wide compositional range. The extreme values of silica range from ~44 wt.% in clay phyllite (Garzón et al., 2016) up to 84 wt.% in quartz phyllite (Saupé and Vegas, 1987). Also Al_2O_3 contents vary from as low as 8.85 wt.% in quartz phyllite (Saupé and Vegas, 1987) to 27 wt.% (Garzón et al., 2016). Calcium is typically very low in phyllites (<1 wt.%) except for carbonate-rich varieties. For instance, some phyllites from southern Spain contain >30 wt.% dolomite (Garzón et al., 2016). Sodium and potassium vary considerably in phyllites from various localities. Iron predominates over magnesium with few exceptions (e.g., Rasul, 1963; Opara et al., 2014).

Modal analyses of phyllites are rather scarce; nevertheless, from the existing data it is clear that the chemical composition of phyllites is directly related to the mineral composition, namely to the amount of quartz, feldspars and phyllosilicates (excluding carbonate-rich phyllites). Based on the proportion of the amount of phyllosilicates to silt fraction (quartz and feldspars), phyllites can be grouped into argillaceous and silt-rich varieties. For the purpose of this paper, we will consider argillaceous phyllites as those with at least 40 wt.% phyllosilicates. The reason for this limit is that there are no phyllites with the predominance of phyllosilicates, i.e. containing >50 wt.% phyllosilicates, reported in the literature. For instance, among 52 phyllite samples from various localities in southern Spain only four contain >40 wt.% phyllosilicates and none >50 wt.% (Garzón et al., 2016). Phyllite samples from the Dewon Quarry are mostly argillaceous (the amount of phyllosilicates ranges from 47 to 55 wt.%) except for the silt-rich JN6 sample (28 wt.% phyllosilicates). As a result, argillaceous phyllites from the Dewon Quarry show elevated content of alumina (19.5 to 20.6 wt.% Al_2O_3) and moderate concentration of silica (52.7 to 55.5 wt.%).

Argillaceous phyllites from the Dewon Quarry are highly enriched in iron compared to phyllites from other localities worldwide (Fig. 7). Iron does not come from secondary iron hydrooxides, since only non-weathered samples were analysed. Despite being highly ferruginous, phyllites from the Dewon Quarry have the Fe/(Fe + Mg) ratio (on average 0.8; Table 2) lower than numerous less ferruginous phyllites from S Spain (Fig. 7) due to relative Mg enrichment of muscovite (Table 2).

The chemical and mineralogical compositions of phyllites reflect clay-rich precursor rocks. Similarity of the chemical compositions of argillaceous phyllites to pelagic pelite (Table 2) suggests the latter as a protolith. This is further confirmed by biomarkers that survived metamorphic conditions and are indicative of bacterial degradation of primary planktonic organic matter suspended in a relatively high water column (pelagic environment). The amorphous organic matter disseminated within the investigated phyllite has features typical of marine sedimentation under anoxic conditions. Those anoxic conditions persisted during metamorphism as suggested by the predominance of divalent iron in phyllosilicates. Hydrothermal activity leading to the precipitation of sulphides in quartz and quartz-albite veins crosscutting phyllite foliation occurred in the reducing environment.

The P-T conditions of metamorphism in the Dewon–Pokrzywna phyllite deposit are difficult to constrain. The tempera-

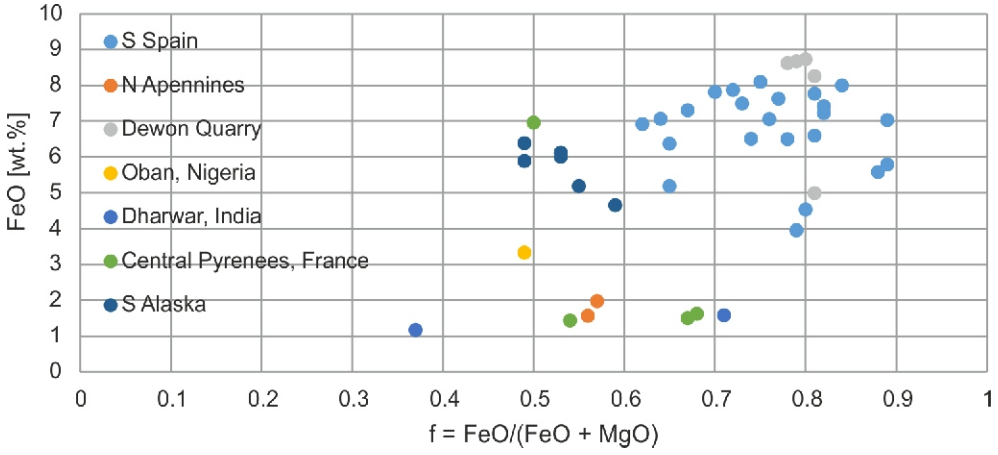

Fig. 7. Plot of f = FeO/(FeO + MgO) (molar ratio) vs. FeO (wt.%) in phyllites from various localities worldwide: S Spain (Garzón et al., 2016), N Apennines, Italy (Lo Pò et al., 2016), Dewon Quarry (this study), Oban, Nigeria (Opara et al., 2014), Dharwar, India (Rasul, 1963), Central Pyrenees, France (Saupé and Vegas, 1987), S Alaska (Gasser et al., 2012)

ture range (~240 to 370°C) estimated from various chlorite geothermometers is too broad to be considered reliable. However, the low temperature of metamorphic processes is suggested by the occurrence of aliphatic hydrocarbons in the phyllite matrix. Therefore, considering mineral assemblages, chlorite geothermometry, and the persistence of aliphatic hydrocarbons we conclude that phyllites in the Dewon–Pokrzywna deposit originated under low-temperature greenschist to high-temperature subgreenschist facies conditions.

Based on thermodynamic modelling and on observations of the deformational microstructure of quartz, Lo Pò et al. (2016) estimated the metamorphic conditions for the formation of phyllites in the Northern Apennines at 300–400°C and 2–7 kbar. Such a broad range of P-T values reflects uncertainties in obtaining reliable data constraining the formation of phyllites.

Argillaceous phyllites from the Dewon Quarry are compositionally comparable to phyllites from Western Saxony that were used in experimental studies on the sorption properties (Arnold et al., 1998). The amount of chlorite and muscovite in those phyllites is 45 vol% and the chlorite to muscovite ratio is 1.25. Saxonian chlorites are less ferruginous than chlorites from the Dewon Quarry with Mg slightly predominating over Fe^{2+} (Fe/(Fe + Mg) = 0.48; Arnold et al., 1998). The increased amount of iron in chlorites, as in the case of phyllites from the Dewon Quarry, is advantageous from the perspective of phyllite sorption behaviour, because chlorite dominates the sorption of uranium onto phyllite indirectly through its weathering to highly sorptive Fe^{3+}-oxyhydroxides (Arnold et al., 1998, 2001). Therefore, Fe^{2+}-rich chlorites have higher potential for being the source of ferric iron, which may precipitate as FeOOH. This has already been shown in the study of chlorites from the Koongara uranium deposit in Australia (Murakami et al., 1996). The average Fe/(Fe + Mg) ratio for those chlorites is 0.53, slightly lower than the mean value of 0.57 for chlorites investigated in this study. The weathered Koongara chlorites underwent vermiculization and during that process Fe^{2+} was oxidized, released, and precipitated as Fe^{3+}-minerals (Murakami et al., 1996). Besides sorption, the direct precipitation of secondary uranium minerals on Fe-ripidolite was shown to be another mechanism for immobilization of migrating actinides (Eberly et al., 1996). By analogy, Fe-ripidolite in phyllites from the Dewon–Pokrzywna deposit may also have high immobilizing capability, although its BET specific surface area is lower than of smectites.

Low volume of interconnected pores in phyllites, determined in this study, and the predominance of mesopores suggest low permeability of the rocks. Low permeability and high sorption capacity are essential for the proper and long-lasting performance of engineered barriers in radioactive waste repositories. Moreover, the silt fraction of phyllites may also play a useful role in compensating for volume changes of a clay buffer surrounding waste packages caused by bentonite swelling or shrinkage. Currently, sand mixed with bentonite is used for that purpose in majority of programs for radioactive-waste disposal (Sellin and Leupin, 2013). The advantage of phyllite is that not only it will improve mechanical and thermal properties of a buffer around waste canisters but also it will further enhance its sorption capacity. Alternatively, phyllites can be used as a material for backfilling waste disposal vaults. This study shows that phyllite from the Dewon–Pokrzywna deposit is a potential candidate for a buffer and/or backfill material. However, further study is needed to ensure that the investigated phyllites meet the stringent criteria envisioned for either buffer or backfill materials, including sorption properties, hydraulic conductivity, and mechanical and thermal properties.

Acknowledgements. This study was financially supported by the Polish National Science Center (NCN) grant to M. Fabiańska: 2014/15/B/ST10/02281. We thank L. Jeżak for her assistance with EPMA and E. Teper for her assistance with SEM. We are grateful to B. Bagiński, A.S. Venkatesh and D. Więcław for their valuable critical comments that significantly improved the manuscript.

REFERENCES

Arnold, T., Zorn, T., Bernhard, G., Nitsche, H., 1998. Sorption of uranium (VI) onto phyllite. Chemical Geology, **151**: 129–141.

Arnold, T., Zorn, T., Zänker, H., Bernhard, G., Nitsche, H., 2001. Sorption behavior of U(VI) on phyllite: experiments and modeling, Journal of Contaminant Hydrology, **47**: 219–231.

Balan, E., Saitta, A.M., Mauri, F., Calas, G., 2001. First-principles modeling of the infrared spectrum of kaolinite. American Mineralogist, **86**: 1321–1330.

Bray, E.E., Evans, E.D., 1963. Distribution of *n*-paraffins as a clue to recognition of source beds. Geochimimica et Cosmochimica Acta, **22**: 2–15.

Bucher, K., Grapes, R., 2011. Petrogenesis of Metamorphic Rocks. Springer, Berlin, Heidelberg.

Cathelineau, M., 1988. Cation site occupancy in chlorites and illites as a function of temperature. Clay Minerals, **23**: 471–485.

Clifton, C.G., Walters, C.C, Simoneit, B.R.T., 1990. Hydrothermal petroleums from Yellowstone National Park, Wyoming U.S.A. Applied Geochemistry, **5**: 169–191.

Cooper, B.S., 1990. Practical Petroleum Geochemistry. Robertson Scientific Publications, London.

Da Silva Nogueira de Matos, J.H., Saraiva dos Santos, T.J., Soares Monteiro, L.V., 2017. The carbonaceous phyllite rock-hosted Pedra Verde copper mine, Borborema province, Brazil: stable isotope constraints, structural control and metallogenic evolution. Journal of South American Earth Sciences, **80**: 422–443.

Daniels, K.A., Harrington, J.F., Zihms, S.Z., Wiseall, A.C., 2017. Bentonite permeability at elevated temperature. Geosciences, **7**, doi: 10.3390/geosciences7010003

De Caritat, P., Hutcheon, I., Walshe, J.L., 1993. Chlorite geothermometry: a review. Clays and Clay Minerals, **41**: 219–239.

Didyk, B.M., Simoneit, B.R.T., Brassell, S.C., Eglington, G., 1978. Organic geochemical indicators of palaeoenvironmental conditions of sedimentation. Nature, **272**: 216–222.

Eberly, P.O., Ewing, R.C., Janeczek, J., Furlano, A., 1996. Clays at the natural nuclear reactor at Bangombe, Gabon: migration of actinides. Radiochimica Acta, **59**: 271–275.

Garzón, E.G., Sánchez-Soto, P.J., Romero, E., 2010. Physical and geotechnical properties of clay phyllites. Applied Clay Science, **48**: 307–318.

Garzón, E.G., Ruíz-Conde, A., Sánchez-Soto, P.J., 2012. Multivariate statistical analysis of phyllite samples based on chemical (XRF) and mineralogical data by XRD. American Journal of Analytical Chemistry, **3**: 347–363.

Garzón, E.G., Romero, E., Sánchez-Soto, P.J., 2016. Correlation between chemical and mineralogical characteristics and perme-

ability of phyllite clays using multivariate statistical analysis. Applied Clay Science, **129**: 92–101.

Gasser, D., Bruand, E., Rubatto, D., Stüwe K., 2012. The behaviour of monazite from greenschists facies phyllites to anatectic gneisses: an example from the Chugach Metamorphic Complex, southern Alaska. Lithos, **134–135**: 108–122.

ISO 9277:2010. Determination of the specific surface area of solids by gas adsorption – BET method. https://www.iso.org/standard/44941.html

Krakow, L., 2014. Resource efficiency in the clay brick and tile industry Part IX: Slate flour from phyllite sizing. Ziegelindustrie International. Brick and Tile Industry International. Issue **6** at http://www.zi-online.info/en/issue/zi_2014-06_1925050.html

Krawczyk-Bärsch, E., Arnold, T., Schmeißer, N., Brandt, F., Bosbach, D., Bernhard, G., 2004. Formation of secondary Fe-oxyhydroxide phases during the dissolution of chlorite – effects on uranium sorption. Applied Geochemistry, **19**: 1403–1414.

Kříbek, B., Sýkorová I., Machowič, V., Laufek, F., 2008. Graphitization of organic matter and fluid-deposited graphite in Palaeoproterozoic (Birimian) black shales of the Kaya-Goren greenstone belt (Burkina Faso, West Africa). Journal of Metamorphic Geology, **26**: 937–358.

Leythauser, D., Schwartzkopf, Th., 1985. The pristane/*n*-heptadecane ratio as an indicator for recognition of hydrocarbon migration effects, Organic Geochemistry, **10**: 191–197.

Lo Pò, D., Braga, R., Massone, H.-J., 2016. Petrographic, mineral and pressure-temperature constraints on phyllites from the Variscan basement at Punta Bianca, Northern Apennines, Italy. Italian Journal of Geosciences, **135**: 489–502.

Melo, L.G.A., Pires, E.F.G., Pereira, R.A., Silva, F.J., 2017. Physicochemical characterization of pulverized phyllite rock for geopolymer resin synthesis. Materials Research. Doi: http://dx.doi.org/10.1590/1980-5373-MR-2016-0968

Murakami, T., Isobe, H., Sato, T., Ohnuki, T., 1996. Weathering of chlorite in a quartz-chlorite schist: I. Mineralogical and chemical changes. Clays and Clay Minerals, **44**: 244-256.

Opara, K.D., Obioha, Y.E., Onyekuru, S.O., Okereke, C., Ibeneme, S.I., 2014. Petrology and geochemistry of basement complex rocks in Okom-Ita area, Oban massif, Southeastern Nigeria. International Journal of Geosciences, **5**: 394–407.

Oruzinsky, V., Kribek, B.K., 1981. Metamorphosed stratiform Cu-deposit of Tisova (Czechoslovakia). Mineralia Deposita, **16**: 437–442.

Peters, K.E., Walters, C.C., Moldowan, J.M., 2005. The Biomarker Guide. Biomarkers and Isotopes in Petroleum Exploration and Earth History. Cambridge University Press, Cambridge.

Philp, R.P., 1985. Fossil Fuel Biomarkers. Application and Spectra. Elsevier, Amsterdam.

Polish Nuclear Power Programme, 2014. Ministry of Economy. Warszawa (access: http://www.paa.gov.pl/sites/default/files /PPEJ%20eng.2014.pdf)

Rasul, S.H., 1963. The chemical composition and original nature of the Dharwar phyllites of the Shivrajpur-Bamankus area, district Panch Mahals, Gujarat state. Proceedings of the Indian Academy of Sciences – Section A, **58**: 343–351.

Richter, C., Müller, K., Drobot, B., Steudtner, R., Großmann, K., Stockmann, M., Brendler, V., 2016. Macroscopic and spectroscopic characterization of uranium(VI) sorption onto orthoclase and muscovite and the influence of competing Ca^{2+}. Geochimica et Cosmochimica Acta, **189**: 143–157.

Rieder, M., Cavazzini, G., D'Yakonov, Y.S., Frank-Kamenetskii, V.A., Gottardi, C., Guggenheim, S., Koval, P., Muller, G., Radoslovich, E.W., Robert, J.-L., Sassi, F.P., Takeda, H., Weiss, Z., Wones, D.R., 1998. Nomenclature of the micas. The Canadian Mineralogist, **36**: 41–48.

Sahoo, P.R., Venkatesh, A.S., 2014. 'Indicator' carbonaceous phyllite/graphitic schist in the Archean Kundarkocha gold deposit, Singhbhum orogenic belt, eastern India: implications for gold mineralization *vis-a-vis* organic matter. Journal of Earth System Science, **123**: 1693–1703.

Saupé, F., Vegas, G., 1987. Chemical and mineralogical compositions of black shales (Middle Palaeozoic of the Central Pyrenees, Haute-Garonne, France). Mineralogical Magazine, **51**: 357–369.

Sawicki, L., 1955. Szczegółowa mapa geologiczna Sudetów (in Polish). Arkusz M33-71 Bb Głuchołazy.

Sellin, P., Leupin, O.X., 2013. The use of clay as an engineered barrier in radioactive-waste management – a review. Clays and Clay Minerals, **61**: 477–498.

Shahwan, T., Erten, H.N., 1999. Radiochemical study of Co^{2+} sorption on chlorite and kaolinite. Journal of Radioanalytical and Nuclear Chemistry, **241**: 151–155.

Shanmugam, G., 1985. Significance of coniferous rain forests and related organic matter in generating commercial quantities of oil, Gippsland Basin, Australia. AAPG Bulletin, **69**: 1241–1254.

Słomka, T., Doktor, M., Bartuś, T., Mastej, W., Łodziński, M., 2009. Geotourist attractions of the Eastern Sudetic Geostrada (in Polish with English summary). Geoturystyka, **4**: 61–72.

Stańczak, G., 2016. Slates, phyllites and schists from deposits of SW Poland used as dimension stones – evaluation of their decorativeness and the possibilities of use (in Polish with English summary). Przegląd Geologiczny, **64**: 833–843.

Strzyżewska-Konieczna, S., Żaba, J., 2002. Folds and the sequence of deformation of the Andelska Hora unit (Opava Mountains, Eastern Sudetes) (in Polish). Przegląd Geologiczny, **50**: 1221–1222.

Summons, R.E., Powell, T.G., Boreham, Ch.J., 1988. Petroleum geochemistry of the Middle Proterozoic McArthur Basin, Northern Australia: III. Composition of extractable hydrocarbons. Geochimica et Cosmochimica Acta, **52**: 1747–1963.

Tischendorf, G., Förster, H.-J., Gottesmann, B., Rieder, M., 2007. True and brittle micas: composition and solid solution series. Mineralogical Magazine, **71**: 285–320.

Tissot, B.P., Welte, D.H., 1984. Petroleum Formation and Occurrence, 2nd Edition. Springer-Verlag Telos, Berlin.

Wiewióra, A., Weiss, Z., 1990. Crystallochemical classifications of phyllosilicates based on the unified system of projection of chemical composition: II. The chlorite group. Clay Minerals, **25**: 83–92.

Wiley, 2014. NBS Registry of Mass Spectral Data. New York, Wiley.

Vernon, R.H., 2004. A practical guide to rock microstructures. Cambridge University Press.

Van Zuilen, M.A., Lepland, A., Teranes, J., Finarelli, J., Wahlen, M., Arrhenius, G., 2003. Graphite and carbonates in the 3.8 Ga old Isua Supracrustal Belt, southern West Greenland. Precambrian Research, **126**: 331–348.

Yavuz, F., Kumral, M., Karakaya, N., Karakaya, M.Ç., 2015. A Window program for chlorite calculation and classification. Computers & Geosciences, **81**: 101–113.

Zänker, H., Hüttig, G., Arnold, T., Nitsche, H., 2006. Formation of iron-containing colloids by the weathering of phyllite. Aquatic Geochemistry, **12**: 299–325.

Żaba, J., Ciesielczuk, J., Malik, K., Strzyżewska-Konieczna, S., 2005. Structure and structural evolution of the Devonian-Carboniferous rocks of the Opava Mountains (Moravian-Silesian zone) (in Polish). In: Geologia i zagadnienia ochrony środowiska w regionie górnośląskim (eds. J. Jureczko, Z. Buła and J. Żaba): 116–127. LXXVI Zjazd naukowy Polskiego Towarzystwa Geologicznego, Rudy k/Rybnika, 14–16 września 2005.